論 文 33～6～2

ZnO Varistor의 Tunneling Breakdown 특성에 관한 연구

A Study on Tunneling Breakdown Behaviors in ZnO Varistor

池 哲 根*·呉 明 煥**·安 鍾 爀***
(Chol-Kon Chee · Myung-Hwan Oh · Chong-Hyuk Ahn)

요 약

본 논문은 Levinson과 Mahan의 이론을 도입하여 Breakdown 영역에서 산화아연을 주성분으로 한 바리스터의 현저한 비직선 전압—전류 특성에 관해서 이론적으로 해석코져하였다. 산화아연 입자사이의 Junction에 설정된 쌍공핍층 모델을 가지고, 전자의 턴넬이 Breakdown 현상 발생의 주요한 원인이 된다는 것을 이론 및 실험적으로 검토하였다.

이론 및 실험적인 해석으로부터 비직선 지수 α는 ~50이고, 전류밀도 1mA/㎠일때 단위입계의 Breakdown 전압은 대략 2－3V임을 얻었다.

이와같은 결과에 따라 Breakdown 영역에서 ZnO 바리스터의 Breakdown 특성을 설명하는데 전자의 턴넬 Mechanism이 적절하다는 결론을 얻었다.

Abstract

This paper aims at a theoretical explanation of the highly nonlinear voltage-current (V-I) characteristics of ZnO varistors in the breakdown region with the aid of the theory of Levinson[3] and Mahan.[5]

From the double depletion layer model idealized at the junctions between ZnO grains, it is discussed theoretically and experimentally that electron tunneling is predominantly responsible for the breakdown phenomena.

It is shown from the results of experimental and theoretical analysis that a coefficient of nonlinearity α is ~50 and breakdown voltage per grain junction at 1 mA/cm^2 is about 2~3 (V).

Based on these results, it is concluded that in the breakdown region a mechanism of electron tunneling is relevant to explain breakdown behaviors of the ZnO varistor.

I. Introduction

It has been reported that the zinc-oxide (ZnO) ceramics with additives such as Bi_2O_3, MnO, CoO, Sb_2O_3, Cr_2O_3 show highly nonlinear voltage-current (V-I) characteristics.[1)-4)]

Several theoretical models[5)-7)] have been proposed to explain the nonlinear voltage-current relationships and conduction mechanisms in the breakdown region.

However, none of them gives a satisfactory and quantitative explanation of the observed varistor behaviors in the breakdown region, and it remains as a problem to be solved.

This paper aims at a possible explanation for electrical breakdown behaviors of the ZnO varistor in the operating region with the aid of the theory of Levinson[3] and Mahan.[5]

*正會員：서울大 工大 電氣工学科 教授·工博
**正會員：韓国科学技術院 計測素子研究室 室長·工博
***正會員：仁川専門大学 電子計算科 専任講師
接受日字：1984年 2月 6日

Our plausible explanations may be applicable to predict the voltage-current characteristics even when the variable factors are changed in the fabrication of ZnO varistors.

II Experimental Procedure and Results

II-1 Materials and Processing

Mixtures ZnO with additives 0.75 mol % (Bi_2O_3+MnO+CoO+2Sb_2O_3+Cr_2O_3) in a chemical reagent grade of 99.0% purity were used.

Mixtures of these materials were calcined in the air at 700°C for an hour, and pressed into discs of 10mm in diameter and 2mm in thickness at a pressure of 1500kg/cm^2.

These discs were sintered in an alumina tube furnace in the air.

The furnace temperature was raised at a rate of 300°C per hour, kept at a constant temperature of 1275°C for an hour and then furnace cooled.

The disc thickness was shrunk to 1.8mm after sintering.

The sintered discs were lapped with a silicon carbide abrasive and ohmic contacts were made on either surface using aluminum.

A simplified flow diagram of fabrication of ZnO varistors is shown in Fig. 1.

II-2 Measurement of Voltage-Current Characteristics

The voltage-current characteristics of non-ohmic ZnO varistor are expressed approximately by

$$I = KV^{\alpha}, \qquad (1)$$

where V is the voltage across the sample, I is the current flowing through the sample, K is the constant, and the parameter α [=d (logI)/d (log V)] is a measure of the device nonlinearity.

The V-I curves were measured by using D.C. power supply in a current range up to 10 mA.

In the high current range above 10mA, the measurement was carried out by applying a single pluse of 8/20 μs exponential wave shape to avoid unnecessary joule heating.

II-3 Experimental Results

Fig. 2 shows the typical V-I curves obtained

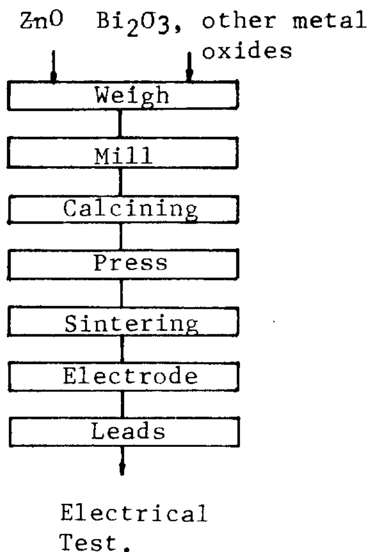

Fig. 1. Simplified flow diagram for the fabrication of ZnO varistors.

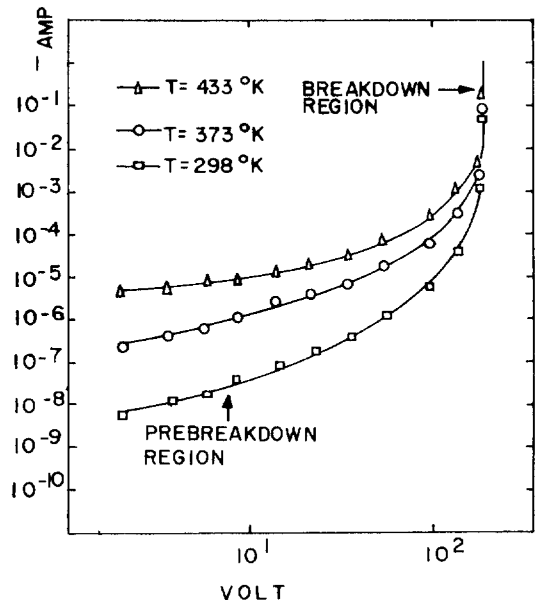

Fig. 2. Current-Voltage characteristics of a Zno varistor at various temperature.

at various temperatures and it can be observed that the V-I curve below at a certain voltage has a large temperature dependence, whereas the V-I curve at the region above this voltage has a small temperature dependence.

Analysis of these experimental results shows that in the prebreakdown region the current flow phenomena may be caused by thermal excitation of the electrons over the barrier, while in the breakdown region the rapid current rise might be caused by some electronic tunneling phenomena through the barrier.

III. Theoretical Considerations

III-1 Calculation of Intergranular Layer Thickness

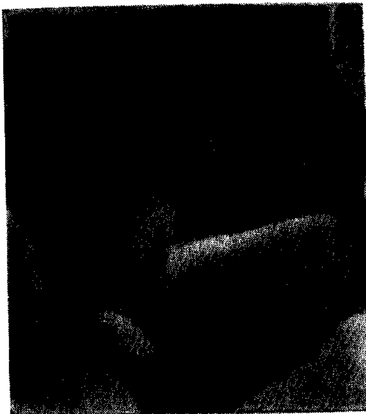

Fig. 3. Scanning electron micrograph taken on the surface area of ZnO varistor.

As shown in Fig. 3 and Fig. 4 it seems that the ZnO varistor has a microstructure which has segregated ZnO grains by thin intergranular layer with grainboundary interface, having a depletion layer.

The current may flow from ZnO grain to the interface, and then on to the next ZnO grain.

Here we assume that ZnO grains are cubes with uniform side d, the intergranular layer of insulator being of uniform thickness t, as the

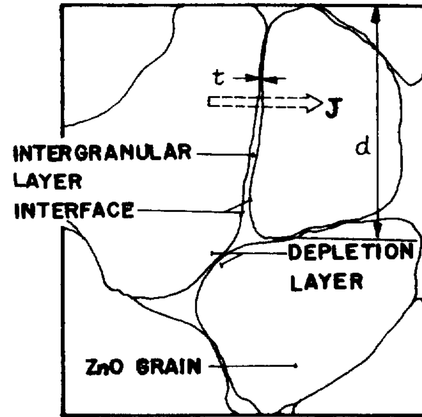

Fig. 4. Analogical depiction of scanning electron micrograph.

profile of idealized microstructure of ZnO varistors.

By using the idealized microstructure, we obtain the relation as

$$\frac{\text{Volume (additives)}}{\text{Volume (total)}} \approx \frac{3t}{d} \approx \text{additive mole } \%, \quad (2)$$

provided $d \gg t$,

where d and t are the average diameter of ZnO grains and the thickness of intergranular layer respectively.

In the breakdown region, we have obtained the result that the nonlinearity α is about 50 from Eq.(1).

From the profile of idealized microstructure, we can also estimate the number of grains between electrodes, and then obtain a breakdown voltage at 1mA/cm^2 of 2-3 V/grain.

And, therefore, we can estimate the thickness t of intergranular layer about 80Å~200Å for $d=10\sim25\mu$ from Eq.(2), which may be compared with the data obtained by other workers.[9)-10)]

Even though the actual thickness of intergranular layer is quite variable in this polycrystalline ceramics, we can assume that the thinnest interfacial area below 100Å in thickness must be responsible for electronic transport phenomena in this ZnO varistor.

III-2 Calculation of the Activation Energy

In the prebreakdown region of Fig. 2, the voltage-current characteristics exhibits an obvious temperature dependence, whose negative temperature coefficient indicates that ZnO varistor has some thermionic emission behaviors of semiconductive material.

Therefore, from the modified relationships of Schottky emission,

$$J=J_1 \exp[-(\phi_B-BF^{1/2})/KT], \qquad (3)$$

where J, ϕ_B, F, B and J_1 indicate current density, activation energy, applied electric field, Poole-Frenkel coefficient[11] and a constant respectively.

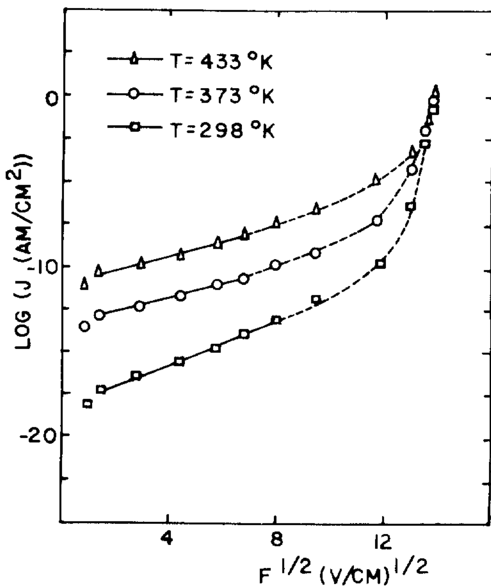

Fig. 5. V-I relationships in the prebreakdown region (The straight line corresponds to the intrinsic behaviors of field-assisted thermal emission).

And also from the linear relationship between ℓnJ and $F^{1/2}$, 1/T plotted in Fig. 5 and Fig. 6, we obtain

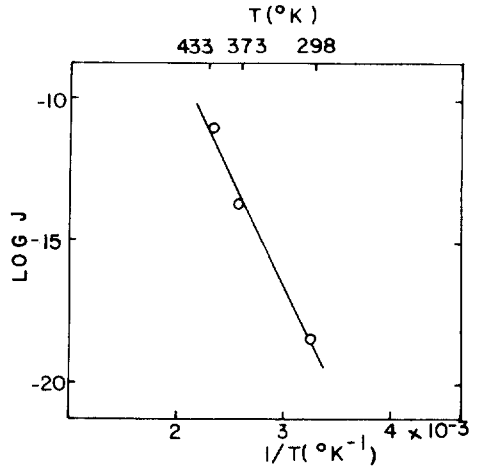

Fig. 6. Plot of ℓn J against inverse temperature (extrapolated to F=O using Fig. 5).

$$\phi_B=K\frac{\ell nJ_2-\ell nJ_1}{1/T_2-1/T_1}. \qquad (4)$$

The activation energy, ϕ_B=0.73(ev), can then be found from Fig. 6 and Eq.(4).

Though the actual activation energy is a function of externally applied field and temperature, we assume in this paper that the variation of activation energy is negligible.

III-3 Analysis of the Conduction Phenomena

As many workers have done,[5),6),9)] we have examined the possible electrical conduction mechanism in our own varistor model.

A quantitative approach to two-step transport of electronic carriers through the formulated potential barrier shows a good agreement between theoretically calculated and experimentally obtained V-I relationships.

III-3-1 Formulation of Potential Barrier Models

We have the double-depletion layer described with the interface between adjacent ZnO grains for an idealized potential barrier model.

The Poisson's equation for the potential

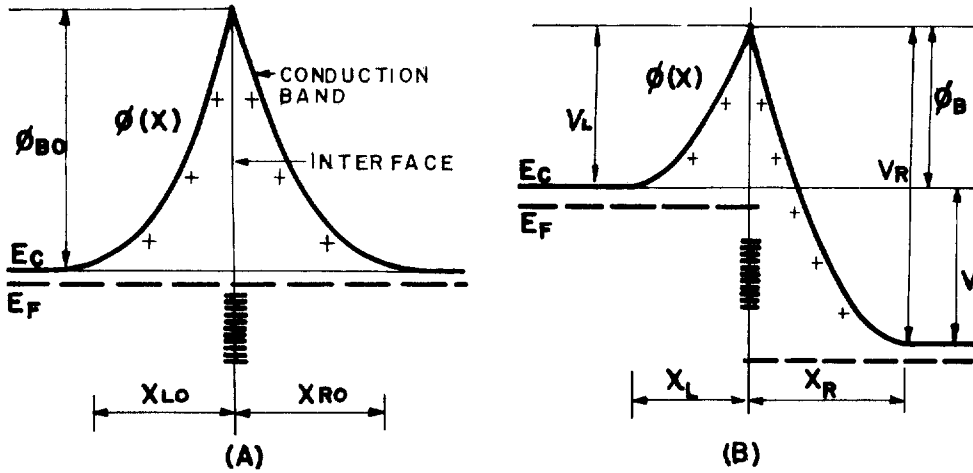

Fig. 7. Sketches of double depletion layers (A) without and (B) with an applied voltage V

barrier function for electron denoted by $\phi(X)$, then $\phi(X)$ is

$$\frac{\partial^2}{\partial X^2}\phi(X) = \frac{4\pi e^2 \eta_0}{\varepsilon_0}, \quad (5)$$

where η_0 and ε_0 are respectively the positive donor density in the depletion region of the ZnO ($\eta_0 \approx 10^{17}\,cm^{-3}$) and the dielectric constant of the ZnO ($\omega_0 \approx 10$)[3].

From the solution of Eq.(5) with following boundary conditions, we have

i) $-X_L \leqslant X \leqslant 0$ (6)

$$\phi(X) = \tfrac{1}{2}\gamma n_0 (X_L + X)^2,$$

ii) $0 \leqslant X \leqslant X_R$ (7)

$$\phi(X) = \tfrac{1}{2}\gamma n_0 (X_R - X)^2 - V,$$

where $\gamma = 4\pi e^2/\varepsilon_0$.

Also from Eqs. (6), (7) and $\phi(0) = \phi_B$, we obtain some useful relations such as:

$$X_L = [\frac{2}{\gamma n_0}\phi_B]^{1/2}, \quad (8)$$

$$X_R = [\frac{2}{\gamma n_0}(\phi_B + V)]^{1/2}, \quad (9)$$

$$V = \tfrac{1}{2}\gamma n_0 (X_R^2 - X_L^2), \quad (10)$$

$$\phi_{BO} = \frac{\pi e^2 n_0}{2\varepsilon_0}(X_{RO} + |X_{LO}|)^2 \quad (11)$$

and $\phi_B(V) = \phi_{BO}\,(1 - \frac{V}{4\phi_{BO}})^2$. (12)

Although both X_L and X_R vary with applied field, their sum must be constant. Thus Eq.(12) is satisfied under the assumption of $|X_{LO}| + X_{RO} = |X_L| + X_R$.

We can understand that the potential barrier height in the left depletion region vanishes at applied voltage $V = 4\phi_{BO}$, so-called critical voltage for varistor breakdown.

This model enables us to predict a critical voltage $V = 4\phi_{BO} \approx 2.9$ (eV) per grain at the breakdown phenomena, which turned out to be 2-3 (eV)[6] in many other cases of experimental results.

We suppose that it could be one of probable model for analysis of our own varistor conduction phenomena.

III-3-2 Two-step Transport

Here, we assume that the electron transfer from ZnO grain to the interface, and then on to the next ZnO grain, are separable into two-step transport as shown in Fig. 8.

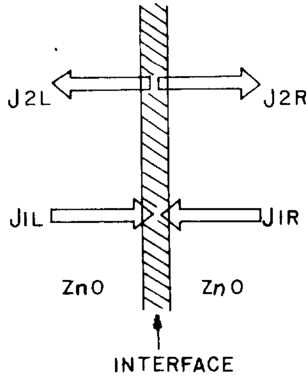

Fig. 8. The two-step model of charge transport.

The current flows from ZnO on to the interface are considered to occur by thermal activation.

The conduction current is given by

$$J_{1L}=J_0 \exp(-\beta V_L), \tag{13}$$

$$J_{1R}=J_0 \exp(-\beta V_R), \tag{14}$$

where $\beta=/KT$.

The currmnt flow from the interface to the ZnO grains is assumed to be proportional to the charge density (σ) in the interface. The current flows are given by

$$J_{2L}=J_{2R}=J_{2\sigma} \exp(-\beta \phi_B). \tag{15}$$

Since the current flow is usually continuous at the interface, we have

$$J_{1L}+J_{1R}=J_{2L}+J_{2R}. \tag{16}$$

From Eq.(16) we obtain the interface charge density as

$$\sigma=\frac{J_0}{2J_2}\{\exp[-\beta(V_L-\phi_B)]+\exp[-\beta(V_R-\phi_B)]\}. \tag{17}$$

The value of J_2 is obtained from the zero-voltage equilibrium condition, where we have $V_L=V_R=\phi_{B0}$ and $\sigma=\sigma_0$:

$$J_2=J_0/\sigma_0 \tag{18}$$

Substituting Eq. (18) in Eq. (17), we obtain the normalized interface charge function (ξ) varied with applied voltage as

$$\xi=\frac{\sigma}{\sigma_0}=\frac{1}{2}[\exp[-\beta(V_L-\phi_B)]+\exp[-\beta(V_R-\phi_B)]]. \tag{19}$$

III-4 The Case of Prebreakdown Region

Let the interface have a normalized charge function $\xi=\sigma/\sigma_0$ which varies with applied voltage and the transport ($J_{2R}+J_{2L}$) from the interface is assumed to be proportional to the amount interface charge σ.

The double depletion layer model at pre-breakdown is shown in Fig. 9.

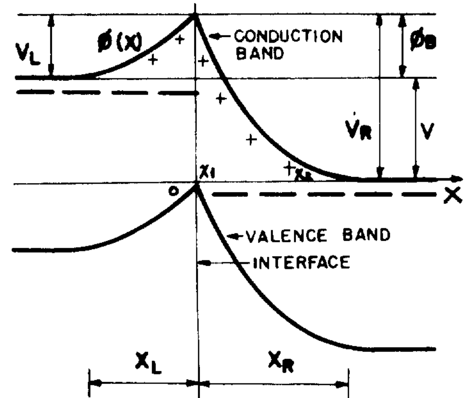

Fig. 9. Sketch of the double depletion layer model at prebreakdown.

When electrons flow to the right, this model shows that the righthand side of ZnO depletion layer becomes thin enough to cause tunneling conduction through it. For the right hand-side electron flow we can modify Eq.(15) for the transport equations from the interface to the ZnO, resulting in

$$J_{2R}=J_0\xi \exp(-\beta\phi_B) Y(V_R), \tag{20}$$

where we have

$$Y(V_R) = \frac{1}{U}\int_0^{\phi B} dE \exp(\beta E) \exp[-W(E, V_R)], \quad (21)$$

$$U = \int_0^{\phi B} dE \exp(\beta E) \exp[-W(E, \phi_B)]. \quad (22)$$

The WKB intergral for tunneling from the interface at an energy E below the top of the interface, as in Fig. 9, is

$$W = 2\int K(X)\, dX$$

$$= 2\left(\frac{2m}{\hbar^2}\right)^{1/2} \int_{X_1}^{X_2} dX[\gamma'\eta_0(X_R - X)^2 - (V_R - E)]^{1/2}. \quad (23)$$

Here we define $\gamma' = \frac{1}{2}\gamma$, $y = (\gamma'\eta_0)^{1/2}(X_R - X)$ as a matter of convenience, and by changing integration variable Eq.(23) expressed in the function of barrier width X can be rewritten in the function of electron energy y.

Thus Eq.(23) may be rewritten as

$$W = 2(2m/\hbar^2)^{1/2} \int_{y_1}^{y_2} dy\left[-\frac{1}{(\gamma'\eta_1)^{1/2}}(y^2 + E - V_R)^{1/2}\right]$$

$$= \frac{4}{\hbar W_p} \int \frac{V_R^{1/2}}{(V_R - E)^{\frac{1}{2}}} dy(y^2 + E - V_R)^{1/2}, \quad (24)$$

where $W_p^2 = 4\pi\eta_0 e^2/\varepsilon_0 m$.

The integral in $Y(V_R)$ covers over the interface energy from the top of the barrier (E=0) down to the Fermi level ($E = \phi B$) in the interface. The factor exp (−W) is the WKB approximation tunneling probability through the barrier, and exp $[-\beta(\phi_B - E)]$ is the probability of thermal excitation of a particle to this energy. The factor U is a normalization integral.

From the two-step transport model, the normalized interface charge function (ξ) may be rewritten as,-

$$\xi = \exp[-\beta(V_L - \phi_B)] \frac{1 + \exp(\beta V)}{1 + Y(V_R)}. \quad (25)$$

In order to calculate the current, we use the following expression for electron flow to the right:

$$J = J_{2R} - J_{1R}$$

$$= J_0 \exp(-\beta\phi_B)\{\xi(Y(V_R) - \exp[-\beta(V_R - \phi_B)]\}$$

$$= J_0\, \xi \exp(-\beta\phi_B)\, Y(V_R) \quad (26)$$

from Eqs. (14) and (20).

For $V_R - \phi_B \gg KT$, the term exp $[-\beta(V_R - \phi_B)]$ in eq.(26) may be ignored.

III-5 The Case of Breakdown Region

We have examined that when the conduction band drops below the top of the valence band on the same side of the junction due to the biased field effects, the highly nonlinear breakdown behaviors of varistors may be caused by hole creation in the ZnO.

At breakdown the depletion layer model is shown in Fig. 10.

Before turning to a consideration of this model, it is worthwhile to consider some details of possible mechanism for creating the holes.

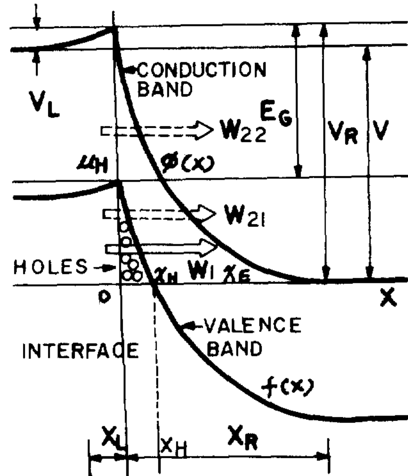

Fig. 10. Deformation of energy band and depletion layer structure at breakdown.

When electrons tunnel from the interface to the conduction band, some will have sufficient kinetic energy to create an electron-hole pair by interband excitation.

The mechanism of creating the hole for ZnO and the efficiency of interband excitation of electron-hole pairs were reported in Ref. 12. For $V_R>\phi_R+E_G$, all of tunneling electrons have sufficient kinetic energy to create the electron hole pairs. But for $E_G<V_R<E_G+\phi_B$, only thermally activated electrons have a sufficient kinetic energy to allow this mechanism.

The onset of hole creation starts at $V_R=E_G$.

It was reported by Levinson[3] and Mahan[5] that this mechanism of creating the hole provides an adequate rate of hole production to explain the build-up of the hole charge necessary for this study.

These holes in turn make the potential barrier much thinner enough to allow electrons tunneling from the interface.

The hole chemical potential in such a case is

$$\mu_H = V_R - E_G. \tag{27}$$

The change of potential shape can be calculated from Poisson's equation expressed as

$$\frac{d^2}{dx^2}\phi(X) = \frac{4\pi e^2}{\varepsilon_0}[\eta_H(X)+\eta_0], \tag{28}$$

where $\eta H(X)$ is the hole charge density. From the Thomas –Fermi approximation,

$$\eta_H(X)=\frac{1}{3\pi^2}\left(\frac{2m}{\hbar^2}\right)^{3/2}(\phi-\mu_H)^{3/2}. \tag{29}$$

Generally, it is very convenient to define a function as

$$f(x)=\phi(X)-\mu_H,$$

where f(x) describes a valence band shape. So Eq.(28) can be rewritten as

$$\frac{d^2}{dx^2}f=\frac{4\pi e^2}{\varepsilon_0}\left[\frac{1}{3\pi^2}\left(\frac{2mf}{\hbar^2}\right)^{3/2}+\eta_0\right] \tag{30}$$

Multiplying by df/dx and integrating gives

$$\frac{\varepsilon_0}{8\pi e^2\eta_0}\left(\frac{df}{dx}\right)^2=b\,f^{5/2}+f+c, \tag{31}$$

where $b=\frac{2}{15}\frac{1}{\pi^2\eta_0}\left(\frac{2m}{\hbar^2}\right)^{3/2}$ and $c=V_R-\mu_H=E_G$

Taking a square root in both sides of Eq.(31) gives

$$\left(\frac{8\pi e^2\eta_0}{\varepsilon_0}\right)^{1/2}\left(\frac{dx}{df}\right)=(bf^{5/2}+f+E_G)^{-1/2}. \tag{32}$$

Integrating from x=0 to $x=x_H$, Eq.(31) becomes

$$(X_H-X)\left(\frac{8\pi e^2\eta_0}{\varepsilon_0}\right)^{1/2}=\int_0^{f(x)}(by^{5/2}+y+E_G)^{-1/2}dy, \tag{33}$$

where $y=(\gamma' n_0)^{1/2}(X_R-X)$.

The value of X_H is found from Eq.(33) at X=0, where we have $f(0)=V_R-E_G$.

Thus

$$X_H=\frac{1}{2(\gamma' n_0)^{1/2}}\int_0^{V_R-E_G}dy\,(E_G+y+by^{5/2})^{-1/2}, \tag{34}$$

where X_H marks the end of the hole region in Fig. (10).

As the potential $\phi(X)$ has a nonparabolic shape in the region of the holes, potential equations become

$$\phi(x)=f(x)+E_G,\quad 0\leqslant X\leqslant X_H,$$
$$\phi(x)=\gamma' n_0(x_R-x)^2,\quad X_H\leqslant X\leqslant X_R. \tag{35}$$

(The potential $\phi(x)$ is continuous and has a continuous derivative at the end of the hole region.

From Eq.(35), we have

$$\phi(X_H)=E_G=\gamma' n_o (x_R-x_H)^2, \qquad (36)$$

$$\left(\frac{df}{dx}\right)_{X_H} = \left[\frac{d}{dx}\gamma' \eta_o (X_R-X)^2\right]_{X_H}$$
$$=-2\gamma' n_o (x_R-x_H)$$
$$=-2(\gamma' n_o E_G)^{1/2}$$

We then have from Eqs.(36), (37) and $\frac{d\phi(X_H)}{dX_H} = \left(\frac{df}{dx}\right)_{X_H}$

$$X_R=X_H+(E_G/\gamma' n_o)^{1/2} \qquad (38)$$

These equations determine X_H and X_R, and the potential shape can be completely specified.

The injected holes will result in a large increase in the positive charge density in the depletion region.

Because of charge neutralization principle, there must exist simultaneously an equal amount of electron charge in the interface.

Thus the model implies that the interface must be charged in order to cancel the positive charge of the holes. Then, the total amount of charge in hole region becomes

$$\eta_T = \int_0^{X_H} dx[n_H(X)+n_o]$$
$$=\frac{\varepsilon_0}{4\pi e^2}\left[\left(\frac{df}{dx}\right)_{X_H}-\left(\frac{df}{dx}\right)_o\right]=-\eta_o X_H. \qquad (39)$$

From Eqs.(19) and (39), and normalized interface charge function(ξ) can be expressed as

$$\xi=\frac{\sigma_T}{\sigma_o}$$
$$=\frac{n_T(X_R-X_L)}{\sigma_o}$$
$$=\frac{(V_R)^{1/2}+(V_L)^{1/2}}{2(\phi_B)^{1/2}\ 2(rn_o)^{1/2}}$$
$$\int_0^{\mu_H} dy(E_G+y+b\, y^{5/2})^{-1/2} \qquad (40)$$

The main difference of this procedure from the precedent is that now $Y(V_R)$ becomes very large in the breakdown region. Note that the former equation Eq.(21) is still useful to evaluate $Y(V_R)$, except that the WKB tunneling integral is different.

We can here suppose two possible situations as the following:

i) for $E<\mu_H$

In this condition, the electron tunnels through a barriers which is determined by the shape derived from Eqs. (30), (34) and (35).

$$W_1(E,V_R)=\frac{2}{\hbar W_p}\int_0^E dy \frac{(E-y)^{1/2}}{[V_R-y+b(\mu_H-y)^{5/2}]^{1/2}} \qquad (41)$$

ii) For $E>\mu_H$

In the case of $E>\mu_H$, the electron tunneling trajectory is partly (W_{21}) in the potential region determined by the holes and partly (W_2^2) in the region with a parabolic conduction band shape, i.e.,

$$W_2=W_{21}+W_{22},$$

where

$$W_{21}=\frac{2}{\hbar W_p}\int_0^{\mu_H} dy \frac{(E-\mu_H+y)^{1/2}}{[E_G+y+by^{5/2})^{1/2}} \qquad (42)$$

and

$$W_{22}=\frac{2}{\hbar W_p}\left[(E_G+E-V_R)^{1/2}(E_G)^{1/2} - (V_R-E)\ell n\left(\frac{(E_G+E-V_R)^{1/2}+E_G^{1/2}}{(V_R-E)^{1/2}}\right)\right]. \qquad (43)$$

Finally, the total current flow through the potential barrier to the right can be obtained from

$$J=J_2R-J_1R$$
$$=J_o\,\xi\exp(-\beta\phi_B)\,Y(V_R). \qquad (44)$$

III-6 Theoretical Results

An approximate calculation for the above mentioned equation can be performed with the condition of $V_R > \phi_{Bo}$ for the interface charge given by Eq. (40).

Computer aided calculations of $Y(V_R)$ and WKB integral show more analytical approximation, where all the physical parameters are typically and already known in ZnO varistor material.

The flow chart of computation is shown in Fig. 11. Here we use the method of Gaussian quadrature in order to calculate the definite integral.

Relationships between theoretically calculated current density vs applied electric field for a single grain junction of ZnO varistor are shown in Fig. 12.

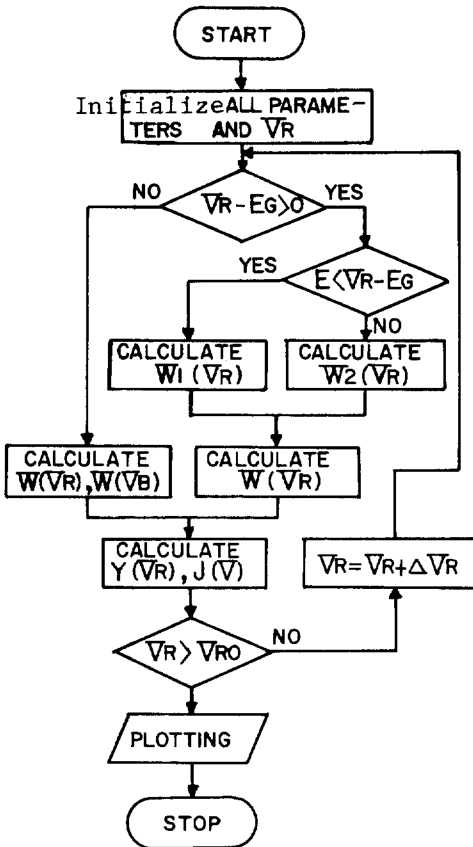

Fig. 11. The flow chart of computation.

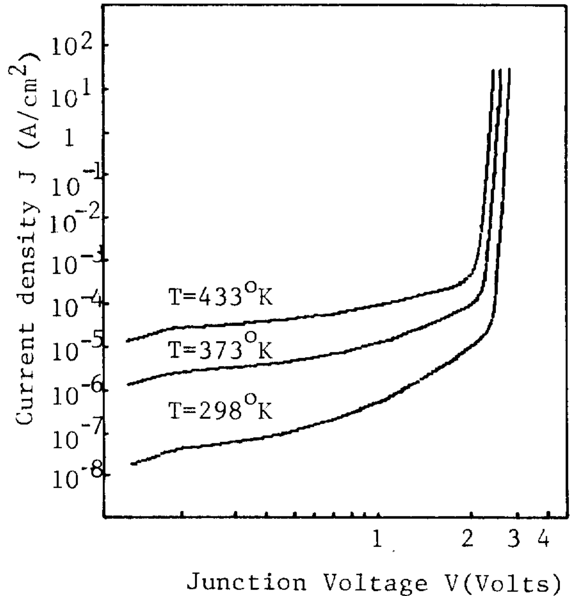

Fig. 12. Current density vs applied electric field for a single grain junction of ZnO varistor.

As shown in Fig. 12, the current rises sharply with applied voltage in the breakdown region and the breakdown voltage at $1\,mA/cm^2$ per junction is about 2-3(V), which is insensitive to the temperature variation.

It can also be shown that in the breakdown region the exponent of nonlinearity α is about 50 from Eq. (1).

We should note that the current density J in Eq. (44) is thermally activated in the prebreakdown region, but not in the breakdown region. When $Y(V_R)$ is dominated by tunneling we have $Y(V_r) \sim \exp(\beta\,\phi_B)$ since the major contribution to the integral in Eq. (21) is at $E=\phi_B$.

Finally, it can also be shown that the quantity $J \propto Y(V_R)\exp(-\beta\,\phi_B) \propto \exp(\beta\,\phi_B)\exp(-\beta\,\phi_B) = 1$ is temperature insensitive in the breakdown region from the approximated numerical evaluations.

IV. Conclusion

Theoretical calculations on the conducting currents vs applied electric fields by use of double depletion model with some depictions of hole creation give us a good agreement with experimental results.

The strong advantages of this theoretical analysis on the conduction mechanisms in our ZnO varistor are the possibilities to describe some identical relationships with actual parameters of nonlinear semiconductive materials as follows:

1) In the breakdown region, the nonlinearity exponent, $\alpha \approx 50$, obtained from the experimental result is corroborated by the result obtained from the theoretical result.
2) Breakdown voltage per grain junction at 1 mA/cm^2 conduction current density is 2-3(V). This is also in agreement with the experimental observations.
3) Varistor leakage currents increase with temperature in the prebreakdown region. It indicates that ZnO varistor has behaviors of thermionic emission in the prebreakdown region.
4) At breakdown a dominant mechanism is the tunneling of electrons through the barrier as confirmed by the theoretical procedures.
5) Finally, a tunneling breakdown mechanism in the ZnO varistor proposed by Levinson and Mahan is relevant to explain breakdown behaviors of the ZnO varistor.

Further studies are necessary to determine the more accurate intergranular thickness and carrier density in the conduction band, etc.

Authors are indebted to Mr. Chung and Mr. Lee, who are research worker in KAIST, for their kind assistance in laborious electrical characterizations.

References

1) M. Matsuoka; "Nonohmic properties of Zinc-Oxide ceramics", Jpn. J. Appl. Phys., Vol.10, No.6, 736 (1971)
2) J.D. Harden et al; "Metal oxide varistor, a new way to suppress transients", Electron., Vol.45, 91 (1972)
3) L.M. Levinson et al; "The physics of metal oxide varistors", J. Appl. Phys., Vol.46, 1332 (1975)
4) 오명환외 ; " ZnO varistor 의 소결온도와 첨가물 혼합비가 전기적 보호 특성에 미치는 영향 ", 대한전기학회지, 31, 53 (1982)
5) G.D. Mahan et al; "Theory of conduction in ZnO varistors", J. Appl. Phys., Vol.50, No.4, 2799 (1979)
6) J. Bernasconi et al; "Zinc oxide based varistors: a possible mechanism", solid state commun., vol. 21, 867 (1977)
7) P.R. Emtage; "The physics of Zinc oxide varistors", J. Appl. Phys., Vol.48, No.10, 1472 (1977)
8) J.G. Simmons; "Generalized formula for the electric tunnel effect between similar electrodes separated by a thin insulating film", J. Appl. Phys., Vol.34, No.6, 1793 (1963)
9) Kazuo Eda; "Conduction mechanism of non-ohmic Zinc oxide ceramics", J. Appl. Phys., Vol.45, No.5, 2964 (1978)
10) J. Wong et al; "Nature of an intergranular thin film phase in a highly nonohmic metal oxide varistor", J. Appl. Phys. Vol. 46, 1827 (1975)
11) W. Vollmann; "Poole-Frenkel Conduction in insulators of large impurity densitys", Phys. Stat. Sol., Vol.22, 195 (1974)
12) G.W. Ludwig et al; J. Electrochem. Soc., Vol. 117, 348 (1970)